19th Australasian Fluid Mechanics Conference
Melbourne, Australia
8-11 December 2014

Transient Flow Structures around a Cubic Building

S.E. Norris[1] and P.J. Richards[1]

[1]Department of Mechanical Engineering
University of Auckland, Auckland 1142, New Zealand

Abstract

The transient flow around the Silsoe 6m cube has been modelled using Large Eddy Simulation, and the calculated mean, standard deviation, maximum and minimum pressure coefficients are found to agree well with published data. Pressures in regions affected by building induced flow structures are found to have a lower standard deviation in the computational model than in full scale, due to the lower free-stream turbulence intensity of LES model. Strong pressure spikes in the pressure histories of taps on the roof and side walls have been analysed using conditional sampling, with the LES model producing histories that agree with full scale. The LES data reveals that these extreme pressures are caused by the formation and shedding of vortices from the windward edge of the roof and side walls.

Introduction

The Silsoe 6m cube, shown in Figure 1, was built to allow the study of wind flow around structures in full scale. The cubic shape was chosen since it represents a simplified building shape, has multiple planes of symmetry, can be rotated to allow the measurement of pressures from different wind angles, and experiences much of the complex flow found on more complex bluff buildings. Richards et al. [1] was the first of a series of papers which have provided full-scale data from the cube, together with analysis of the pressure and flow fields. The original paper contained a limited selection of mean pressure data which has been used as a benchmark for the verification of wind engineering models. These have predominantly been Reynolds Averaged Navier-Stokes (RANS) models, but do include Large Eddy Simulations (LES) by Lim et al. [2] and Detached Eddy Simulations (DES) by Haupt et al. [3]. In two more recent papers [4][5], Richards and Hoxey extended the mean pressure data by providing statistical summaries for the transient pressure records from the pressure taps. In this paper we use LES to model the flow around the cube, in order to understand the flow structures that cause the transient pressure phenomena seen at full scale.

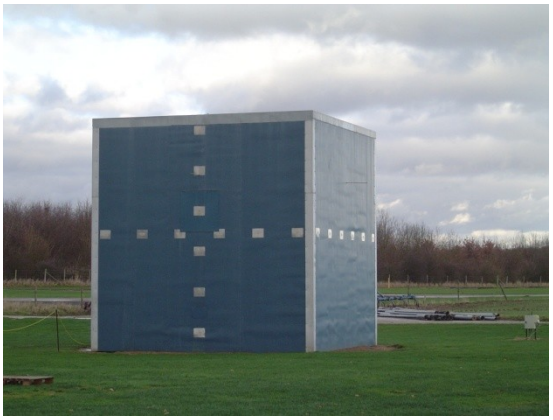

Figure 1. The Silsoe 6m cube, with the location of pressure taps indicated by the grey rectangular patches.

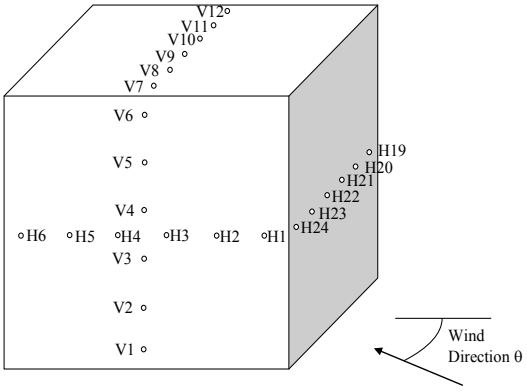

Figure 2. Numbering system used for the pressure taps.

Unsteady Pressure Data

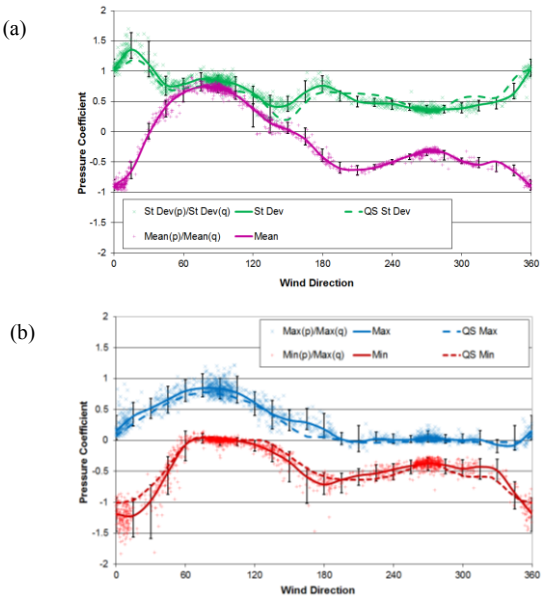

Figure 3. Full-scale pressure coefficients for tap H2, at mid height and 0.24*h* from one vertical edge. (a) Mean and Standard Deviation and (b) Maximum and Minimum pressures.

Shown in Figure 3 are typical full-scale pressure data from the Silsoe cube for one of the mid-height wall taps for a range of flow directions. In each graph the symbols are the data from one 12 minute run, while the solid trend lines are from a Fourier series fitted to the data by using a least squares method. The three dashed lines represent quasi-steady expectations which are derived from the curve fitted to the mean data. A full description of the fitting techniques and quasi-steady modelling are given in [4][5]. It can be seen that the standard deviation and maximum pressure coefficients are approximately equal to that expected from quasi-steady theory; however when the wind direction is in the range 345º-45º the minimum pressure coefficient is consistently more negative than predicted, with the quasi-steady

prediction forming an upper bound to the measured transient data. At this range of angles it is thought that the flow separates from the nearby windward vertical edge and reattaches to the face containing H2 at some point. In [5] it is suggested that these high suction pressures are due to the dynamic response of the separating and reattaching flow which periodically rolls up into an intense vortex. A similar pattern is observed with roof tap V8 when the wind directions is around 90º. The form of the pressure coefficients used here follows [4], where it is recommended that,

$$C_{\bar{p}}(\bar{\theta}) = \frac{\bar{p}}{\bar{q}},\ C_{\tilde{p}}(\bar{\theta}) = \frac{\sigma_p}{\sigma_q},\ C_{\hat{p}}(\bar{\theta}) = \frac{\hat{p}}{\hat{q}} \text{ and } C_{\breve{p}}(\bar{\theta}) = \frac{\breve{p}}{\hat{q}} \quad (1)$$

It has been found that this choice of non-dimensionalisation gives coefficients that are much less sensitive to changes in conditions in comparison with the more usual coefficients, where all pressure statistics are normalised by the mean dynamic pressure.

Numerical Modelling

The simulations were performed using an in-house massively parallel Large Eddy Simulation code, SnS [6],[7], which uses an incompressible non-staggered finite volume formulation based on a structured Cartesian mesh. Second order central differences were employed for approximating the advective and diffusive fluxes in the momentum equations, and an Adams-Bashforth fractional step solver was employed, which gives a solver that has been shown to be second order accurate in both space and time [8]. The fractional step method allows the momentum and pressure equations to be solved in a segregated manner, negating the needs for iterative coupling at each time step, allowing the efficient calculation of transient flows. Subgrid scale turbulence is modelled using the standard Smagorinsky model [9], with wall effects being modelled using the near wall damping model of Mason and Thompson [10] and a rough wall function [11] being applied at the ground boundary.

The majority of calculations were made on a $15h \times 10h \times 6.67h$ computational domain (ie: 90m long, 60m wide and 40m high), using a 246×123×186 mesh with a resolution varying from 0.02m at the wall, to 0.5m in the far field (see Figure 4). The cube was modelled as being aerodynamically smooth, while the ground was modelled with a roughness of $z_0 = 0.01$m. The top of the domain had a free-slip boundary condition applied, and the two side boundaries were modelled as being periodic. The velocity was prescribed at the upstream boundary, having a mean velocity of 6m/s at a height of 6m, and a prescribed pressure outlet boundary condition was applied at the downstream boundary.

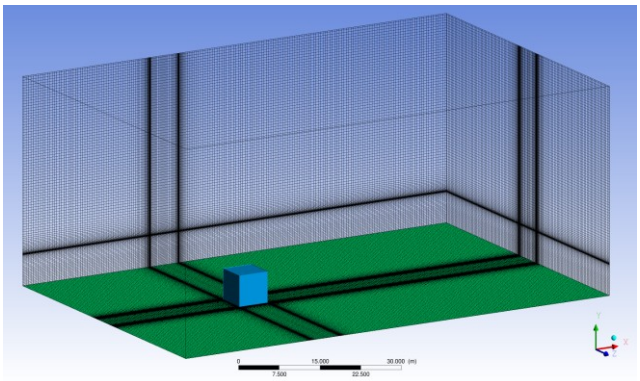

Figure 4. The computational domain. Flow is from left to right.

The inlet boundary condition at the upstream boundary required the definition of an atmospheric boundary layer, including both the mean profile and the temporal and spatial fluctuations of the flow. This was generated using a precursor calculation of the flow in a 720m×40m×60m empty domain with periodic boundary conditions in the streamwise direction, the flow being driven by a pressure gradient in the streamwise direction. The flow at the low x boundary was sampled at 0.05s intervals for a period of 75 minutes. This was broken into 12.5 minute blocks of data, which were used for 6 runs modelling the flow around the cube. The flow was allowed to settle for the first 30s of each run, and then 12 minutes of data was recorded.

The code is parallelised using MPI, and was run on the NeSI Intel Xeon based computational cluster based at the University of Auckland. The momentum equations were solved using a Jacobi solver, with the pressure correction equation being solved using a Bi-Conjugate Gradient Stabilised (BICGSTAB) solver [12] preconditioned using block SIP [13]. When running on 48 cores, 12.5 minutes of simulation time were calculated in approximately 4 days of wallclock time.

It should be noted that the length scale of perturbations in the inlet flow is limited by the use of an incompressible formulation. The mass rate flow through the inlet boundary has to be constant, because the continuity equation requires that any variation in the total inlet flow is matched by an instantaneous change in the flow rate throughout the domain. Therefore large scale gusts with a length scale greater than the domain size cannot be modelled in the inlet turbulence.

Pressure Coefficients and Mean Flow Fields

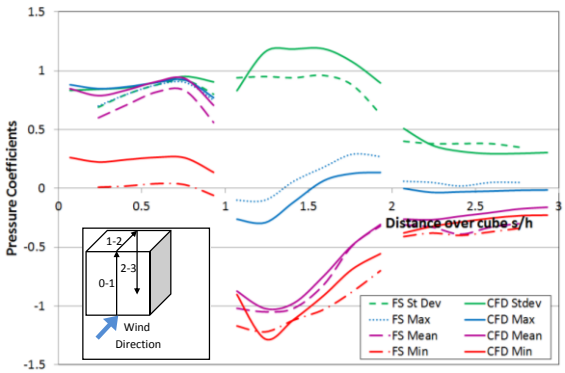

Figure 5. Pressure profiles for the vertical ring for wind direction θ=90º.

Figure 5 shows the pressure coefficient for the vertical ring of pressure taps determined from full-scale measurements and from LES for a wind direction of 90º. The general behaviour of the profiles is matched by the CFD modelling however there are some differences, the most notable being;

- The positive pressures on the windward face are slightly larger in the CFD model.
- The minimum pressures on the windward face are not as low as observed in full-scale. This is probably due to the smaller range of wind directions in the LES runs.
- The maximum pressures on the roof are not as positive as observed in full-scale. This may also be related to the range of wind directions occurring during each 12 minute run. In the LES modelling the lateral turbulence is equivalent to a standard deviation of wind directions of only 3º in contrast to the typical full-scale value of 10º.
- The standard deviation coefficients for the roof are significantly greater in the LES runs than in full-scale. Since the form of pressure coefficient used is the ratio of the standard deviation of the surface pressure to the standard deviation of the reference dynamic pressure, this coefficient is sensitive to the lower level of turbulence that exists in the LES models. The reference longitudinal turbulence intensity in the LES cases was only 9.2% in comparison with typical full-scale values around 19%. This means that any building induced turbulence contributes a greater proportion of the

total standard deviation and hence tends to increase this coefficient.

Short Duration Pressure Spikes

As noted above for tap H2 when the wind angle is near 0º, which is equivalent to tap H8 with wind angle 90º as modelled here, the minimum pressure is more negative than might be expected from quasi-steady analysis. Observation of time histories for the horizontal taps along the side, as illustrated in Figure 6(a), shows that pressure peaks appear to be short duration spikes. The form of these spikes can be clarified by using conditional averaging. Figure 6(b) shows these averages 2s either side of all pressure peaks at tap H8 with a value below -300Pa. A clear sequence of events can be discerned. Just before each peak at H8 a weaker peak is observed at H7, while following the peak at H8 the other side wall taps experience a low suction followed by a rapid change to higher suction. In some cases the pressures at taps H10-12 are positive for short periods during these events. This figure shows that the series of events lasts about 1.5s. The conditionally averaged reference dynamic pressure curve suggests that these peak events may be weakly linked to a gust but do not appear to be immediately triggered by a gust of similar duration. However the fact that the conditionally averaged dynamic pressure is well above the 12 minute average of 126Pa, suggests that the strongest peaks occur during periods of strong winds.

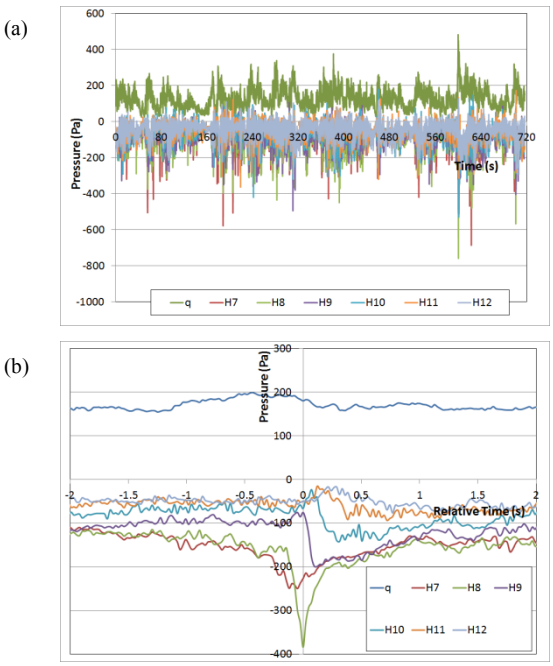

Figure 6. Full-scale pressure data from one 12 minute run during which the wind direction was θ=92.5°; (a) time histories for q and the side pressures and (b) the same pressures conditionally sampled around pressure peaks at H8<-300Pa.

Figure 7(a) shows the time histories for the side wall taps from one LES run. The general behaviour is similar to that in Figure 6(a) although the dynamic pressure is more uniform due to the lower levels of low frequency turbulence in the model. As a consequence the suction spikes at the side wall taps are not as variable in magnitude. The conditional averaged pressure time series triggered by the pressure at tap H8 falling below -35Pa, calculated using all six LES data sets, is shown in Figure 7(b). This reveals a sequence of pressure variations very similar to that seen in full scale. The two most notable differences between the LES data in Figure 7(b) and the full scale data in Figure 6(b) are;

1. The duration of the spike in the LES model is noticeably longer than in the full-scale case. This is probably due to the higher wind speed around the time of the spikes in full-scale (around 16.8 m/s) in comparison with the LES model value (about 5.6 m/s). The observed sequences are thought to be caused by the formation of a tight vortex near the windward edge of the roof or side wall, which is then swept downstream. The speed of movement of the released vortex is likely to be directly proportional to the wind speed.

2. The conditionally averaged dynamic pressure in the LES model are close to the mean value of 19 Pa. This suggests that the spikes in the LES modelling are almost independent of the dynamic pressure whereas the full-scale results suggest that stronger spikes occurred during periods of stronger wind. This observation is related to the inlet turbulence not modelling the long length scale energetic gusts present in the atmospheric boundary layer.

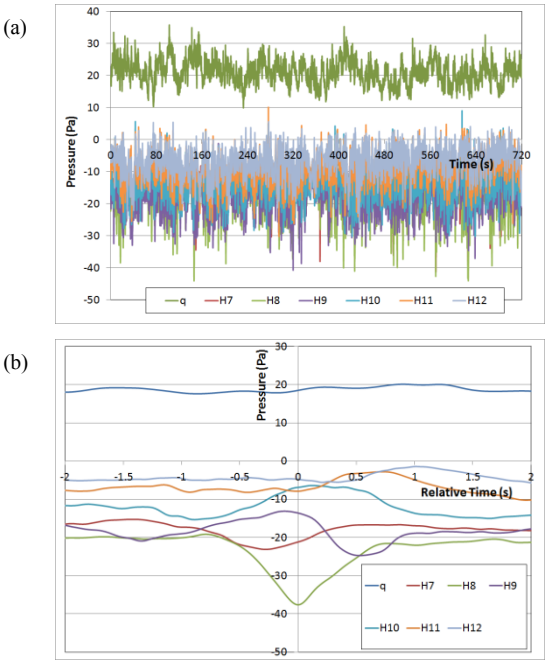

Figure 7. LES pressure data from one 12 minute run during which the wind direction was Θ=90°; (a) time histories for q and the side pressures and (b) the same pressures conditionally sampled around pressure peaks at H8<-35Pa.

Flow Visualisation

Figure 8 reveals the difference in the flow between an instant when the pressure at tap V8, centre of the windward half of the roof, is near its minimum in contrast to that when it is near its maximum. It can be seen in Figure 8(a) that a strong vortex lies over the windward half of the roof resulting in low pressures on this region, as shown by the light coloured area on the windward half of the roof surface. At the same time the pressure colour on the leeward half of the roof is a medium grey indicating neutral and possibly slightly positive pressures. In contrast Figure 8(b) shows a vortex with a horseshoe structure that has lifted off the windward roof surface. The low pressure region on the near side appears to link with a low pressure line on the side wall which runs down towards the windward lower corner at ground level.

Since roof tap V10 has a negative mean and minimum pressure, but a positive maximum, the flow fields have also been extracted for instants when the pressure at V10 is near its maximum and when it is near its minimum. In Figure 9(a) it may be noted that the yellow colour represents a weak positive pressure and there is therefore a small area of positive pressure on the leeward half of the roof at this instant in time. Also at this instant the suction on the windward half is very low and approaches a pressure coefficient of almost -2.0, which is obviously linked to the

intense vortex that exists at this time. It appears that the positive pressure is the result of flow around the vortex impinging onto the surface. In contrast Figure 9(b) shows an instant when the vortex has broken away from the windward edge and is passing over tap V10, lowering the local pressure. However since the core of the vortex appears to have lifted away from the surface the surface pressures are not as low as occurs in Figure 9(a).

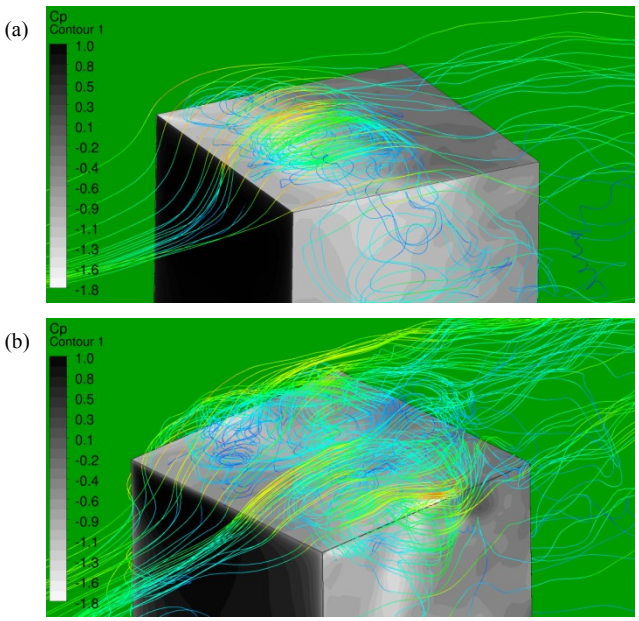

Figure 8. Surface pressures and streamlines at; (a) An instant when the pressure at V8 was near its minimum value, (b) when it was near its maximum.

These flow visualisations support the concept that the pressure sequences observed, both in full-scale and in the LES modelling, result from an intense vortex forming on the windward half of either the roof or side wall. This not only creates high suctions near its core but also weak suctions, and in some cases positive pressures, around its leeward edge. This vortex then breaks free sweeping over the surface creating a positive going pulse followed by a rapid change to a suction pulse. As the vortex moves downstream it lifts away from the surface and so the surface pressures are weaker further downstream.

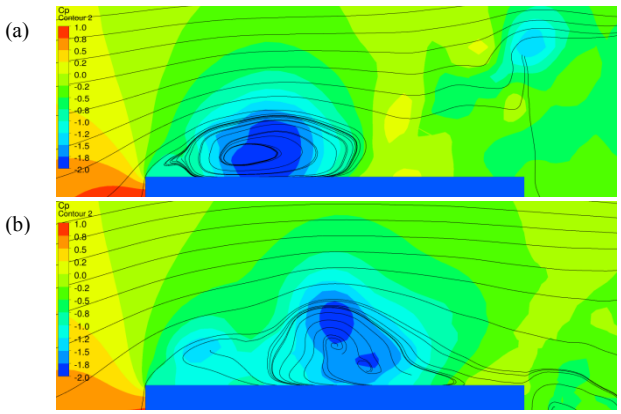

Figure 9. Streamlines and pressure contours on the centre plane when the pressure at V10 is near its (a) maximum and (b) minimum value.

Conclusions

The unsteady flow around the Silsoe cube for a wind direction of 90º, perpendicular to one face, has been modelled using Large Eddy Simulation. The mean, standard deviation, maximum and minimum pressure coefficients for 42 points on the building surface have been compared to published full-scale data and generally good agreement is achieved. In some regions where building induced pressure fluctuations are expected the standard deviation coefficient is higher than in full-scale, probably as a result of the small solution domain which limits the large scale, low frequency turbulence.

The modelling has been used to investigate the suction spikes that occur on the roof and side walls. Conditional averaging was used to highlight the sequence of pressure changes which occurs on the side wall or roof around these high suction events. It is shown that the LES recreates the same phenomena. Flow visualisation shows that the associated velocity field can be characterised as the formation of a strong vortex on the windward half of the side wall or roof, which is then shed and carried downstream.

Acknowledgments

The authors wish to acknowledge the contribution of NeSI high-performance computing facilities to the results of this research.

References

[1] Richards, P.J., Hoxey, R.P. & Short, L.J., Wind pressures on a 6m cube, *J. Wind Eng. Ind. Aerod.*, **89**, 2001, 1553-1564.

[2] Lim, H.C., Thomas, T.G. & Castro, I.P., Flow around a cube in a turbulent boundary layer: LES and experiment, *J. Wind Eng. Ind. Aerod.*, **97**, 2009, 96-109.

[3] Haupt, S.E., Zajaczkowski, F.J., & Peltier, L.J., Detached eddy simulation of atmospheric flow about a surface mounted cube at high Reynolds number. *J. Fluids Eng.*, **133**, 2011, 031002.

[4] Richards, P.J. & Hoxey, R.P., Pressures on a cubic building-Part 1: Full-scale results. *J. Wind Eng. Ind. Aerod.*, **102**, 2011, 72-86.

[5] Richards, P.J. & Hoxey, R.P., Pressures on a cubic building-Part 2: Quasi-steady and other processes. *J. Wind Eng. Ind. Aerod.*, **102**, 2011, 87-96.

[6] Armfield, S.W., Norris, S.E., Morgan, P. & Street, R.A, A Parallel Non-Staggered Navier-Stokes Solver Implemented on a Workstation Cluster, *Proceedings of the Second International Conference on Computational Fluid Dynamics*, 2002, 30–45, Sydney.

[7] Norris, S.E., *A Parallel Navier-Stokes Solver for Natural Convection and Free Surface Flow*. PhD thesis, University of Sydney, 2001.

[8] Armfield, S.W. and Street, R.A., An analysis and comparison of the time accuracy of fractional-step methods for the Navier-Stokes equations on staggered grids, *Int. J. Numer. Meth. Fl.*, **38**, 2002, 255–282.

[9] Smagorinsky, J., General circulation experiments with the primitive equations. *Mon. Weather Rev.*, **91**, 1963, 99–164

[10] Mason, P.J. & Thomson, D.J., Stochastic backscatter in large-eddy simulations of boundary layers. *J. Fluid Mech.*, **242**, 1992, 51–78.

[11] Mason, P.J. & Callen, N.S., On the magnitude of the subgrid-scale eddy coefficient in large-eddy simulations of turbulent channel flow. *J. Fluid Mech.*, **162**, 1986, 439–462

[12] van der Vorst, H.A., Iterative solution methods for certain sparse linear systems with a non-symmetric matrix arising from PDE-problems, *J. Comput. Phys.*, **44**, 1981, 1-19.

[13] Stone, H.L., Iterative solution of implicit approximations of multidimensional partial differential equations, *SIAM J. Numer. Anal.*, **5**, 1968 530-558.